2016

Star Clusters in M31. VII. Global Kinematics and Metallicity Subpopulations of the Globular Clusters

Nelson Caldwell, *Harvard-Smithsonian Center for Astrophysics*
Aaron J. Romanowsky, *San Jose State University*

The Astrophysical Journal, 824:42 (8pp), 2016 June 10 doi:10.3847/0004-637X/824/1/42

STAR CLUSTERS IN M31. VII. GLOBAL KINEMATICS AND METALLICITY SUBPOPULATIONS OF THE GLOBULAR CLUSTERS

Nelson Caldwell[1] and Aaron J. Romanowsky[2,3]
[1] Harvard-Smithsonian Center for Astrophysics, 60 Garden Street, Cambridge, MA 02138, USA; caldwell@cfa.harvard.edu
[2] Department of Physics & Astronomy, San José State University, One Washington Square, San Jose, CA 95192, USA; aaron.romanowsky@sjsu.edu
[3] University of California Observatories, 1156 High Street, Santa Cruz, CA 95064, USA
Received 2016 January 6; accepted 2016 March 21; published 2016 June 8

ABSTRACT

We carry out a joint spatial–kinematical–metallicity analysis of globular clusters (GCs) around the Andromeda Galaxy (M31), using a homogeneous, high-quality spectroscopic data set. In particular, we remove the contaminating young clusters that have plagued many previous analyses. We find that the clusters can be divided into three major metallicity groups based on their radial distributions: (1) an inner metal-rich group ([Fe/H] > -0.4); (2) a group with intermediate metallicity (with median [Fe/H] $= -1$); and (3) a metal-poor group, with [Fe/H] < -1.5. The metal-rich group has kinematics and spatial properties like those of the disk of M31, while the two more metal-poor groups show mild prograde rotation overall, with larger dispersions—in contrast to previous claims of stronger rotation. The metal-poor GCs are the least concentrated group; such clusters occur five times less frequently in the central bulge than do clusters of higher metallicity. Despite some well-known differences between the M31 and Milky Way GC systems, our revised analysis points to remarkable similarities in their chemodynamical properties, which could help elucidate the different formation stages of galaxies and their GCs. In particular, the M31 results motivate further exploration of a metal-rich GC formation mode in situ, within high-redshift, clumpy galactic disks.

Key words: galaxies: individual (M31) – galaxies: star clusters: general – Local Group

Supporting material: machine-readable table

1. INTRODUCTION

Globular star clusters (GCs) have a venerable history as unique tracers of the global properties and formation histories of galaxies, where they can be used as proxies for stellar densities, kinematics, and metallicities over vast scales. The Milky Way (MW) is an archetypal case, where the classic work of Searle & Zinn (1978) inferred from GCs that the outer halo assembled through the protracted infall and merging of smaller galaxies. The MW GC system is currently thought to consist of two or three basic components, with each of them representing a distinct, major mode of ancient star formation (Zinn 1985; Harris 2001). These include an inner component that is flattened, strongly rotating, metal-rich, and identified with the stellar bulge and/or thick disk; and an outer component that is quasi-spherical, weakly rotating, metal-poor, and corresponds to the stellar halo. These halo GCs may be further divided into inner and outer components, sometimes called the "old" and "young" halos, with distinct kinematic and chemical abundance patterns (Mackey & Gilmore 2004; Forbes & Bridges 2010; Keller et al. 2012). Similar divisions have been made in the stellar halo (Carollo et al. 2007; Morrison et al. 2009), with an outer halo interpreted as the debris of satellite galaxies, and an inner halo whose origin is less certain but may have formed "in situ."

It is important to ascertain how general these patterns are for other galaxies, and the natural place to start is our nearest large neighbor, the Andromeda Galaxy (M31). Here there are two broad, well-established differences: (1) the M31 GC system is more populous than the MW system, by a factor of ∼2–3, and (2) it does not exhibit the same obvious bimodality in metallicity (Barmby et al. 2000; Galleti et al. 2009; Caldwell et al. 2011; Cezario et al. 2013). Both of these aspects may be reflections of dramatic differences discovered in these galaxies' stellar halos, where the M31 halo appears much more metal-enriched, with massive substructures suggesting a more active satellite accretion history (e.g., McConnachie et al. 2009).

A third difference has also been noted, involving the rotation. Although early studies of the M31 GC system found relatively weak rotation, particularly among the metal-poor GCs (Huchra et al. 1982; Freeman 1983; Elson & Walterbos 1988; Huchra et al. 1991; Barmby et al. 2000), later studies found stronger rotation (Perrett et al. 2002; Lee et al. 2008; Deason et al. 2011). This is important because the low rotation in the MW is part of the classical line of evidence for accretion in galaxy halos, where myriad minor mergers from quasi-random directions lead to relatively low net angular momentum (e.g., McCarthy et al. 2012). Hence, one natural interpretation of the more recent M31 results is that the rotation traces a past major merger that spun up the entire galaxy (Bekki 2010). However, observations of M31 GCs have historically been fraught with difficulty, owing to interference from its massive, extended disk, leading to false alarms about strong rotation patterns that were actually caused by young disk cluster contamination in the GC sample (as seen in the Perrett et al. 2002; Morrison et al. 2004, and Beasley et al. 2004 papers).

Recent observational efforts have turned to the kinematics of GCs in the outer halo of M31 (beyond ∼30 kpc; Veljanoski et al. 2014), while leaving questions unanswered about the reliability of the previous findings in the inner regions. This aspect may now be addressed through our comprehensive reanalysis of the M31 star cluster system, including both high-quality imaging and a complete spectroscopic data set (Caldwell et al. 2009, 2011, hereafter Papers I and II). In particular, our age determinations allow us to securely differentiate old GCs from young-cluster and foreground-star

Table 1
All Known Globular Clusters in Our M31 Sample

Object	R.A. J2000	decl.	Velocity km s^{-1}	Ref[a]	[Fe/H][b]	Ref[c]	Age[d] Gyr	Log M[e] $M_\odot$	R[f] kpc	R_a[g] kpc
PAndAS-01	23:57:12.0	43:33:08	−333.0±10.0	hx	⋯	⋯	(14)	5.3	117.9	374.1
PAndAS-02	23:57:55.6	41:46:49	−266.0±10.0	hx	⋯	⋯	(14)	5.1	113.7	331.6
PAndAS-04	0:04:42.9	47:21:42	−397.0±10.0	hx	⋯	⋯	(14)	5.2	123.6	409.0
PAndAS-05	0:05:24.1	43:55:35	−183.0±10.0	hx	⋯	⋯	(14)	4.4	99.5	323.5
PAndAS-06	0:06:11.9	41:41:20	−327.0±10.0	hx	−2.1±0.1	pa	(14)	5.6	92.6	268.4
PAndAS-07	0:10:51.3	39:35:58	−452.0±10.0	hx	−1.4±0.2	m13	(14)	4.3	84.9	191.6
PAndAS-08	0:12:52.4	38:17:47	−416.0±10.0	hx	−1.4±0.2	m13	(14)	4.5	87.2	154.3
PAndAS-09	0:12:54.6	45:05:55	−444.0±10.0	hx	⋯	⋯	(14)	5.0	89.8	299.2
PAndAS-10	0:13:38.6	45:11:11	−435.0±10.0	hx	⋯	⋯	(14)	4.5	88.9	296.4
PAndAS-11	0:14:55.6	44:37:16	−447.0±10.0	hx	⋯	⋯	(14)	5.0	82.2	273.8

Notes.
[a] References for velocities: b—Barmby et al. (2000), co—Colucci et al. (2014), p—Perrett et al. (2002), hs2—Hectospec from Paper II, hs7—Hectospec from here; he—Hectochelle from Strader et al. (2011), hx—Huxor et al. (2014) and the references therein; rbc—Galleti et al. (2009).
[b] Minimum uncertainties set to 0.1.
[c] References for [Fe/H]: hs—Hectospec from Paper II or here ("hs7"); c—derived from PHAT colors (N. Caldwell et al. 2016, in preparation); co—Colucci et al. (2014), m06—CMD value from Mackey et al. (2006), m07—CMD value from Mackey et al. (2007) ; m13—CMD value from Mackey et al. (2013) ; pa—CMD value from Huxor et al. (2014), ph—CMD value from PHAT data, (N. Caldwell et al. 2016, in preparation); p11—Perina et al. (2011), r05—CMD value from Rich et al. (2005). Blank where no Hectospec spectroscopy or *HST* CMD exists, and PHAT photometry is not available.
[d] From Paper II. Values in parentheses assigned where no precise age was determined.
[e] Log of total mass, from photometry in Paper II or here.
[f] Radial distance to center of M31.
[g] Defined in the text.

(This table is available in its entirety in machine-readable form.)

contaminants. The new data therefore present an opportunity to review the kinematics of the M31 GC system, and more generally provide an opportunity to carry out a fresh global analysis of its chemodynamical structure, along with a comparison to the MW.

This short paper is structured as follows. In Section 2, we discuss the observational data. In Section 3, we examine the spatial properties of the M31 and MW GC systems. In Section 4, we briefly analyze the kinematic properties of the three major metallicity groups. A more detailed analysis of these trends will be left to future work.

2. M31 OBSERVATIONS, OLD AND NEW

Our M31 GC sample is based on high signal-to-noise spectra from the MMT/Hectospec (Fabricant et al. 2005), which provide not only high-precision velocities (∼6 km s^{-1}), but also secure age and metallicity determinations from high signal-to-noise line indices. This key improvement allowed us to determine more precisely which clusters in our own working catalog (derived originally from the Revised Bologna Catalog Galleti et al. 2007) were indeed old GCs. Another advantage is that the vast majority of our metallicities are on the same system, allowing for a more coherent study of GC subpopulations.[4]

Paper II determined metallicities using iron-dominated Lick indices as measured on Hectospec spectra, with the calibration supplied by similar measurements from the integrated light of Galactic GCs. Those same spectra supplied the velocities used here, supplemented by even more accurate velocities measured in the high dispersion spectra of Strader et al. (2011). These spectroscopically determined metallicities were shown to correspond well to metallicities determined from the color of the red giant branch (RGB) in *Hubble Space Telescope*-produced color–magnitude diagrams (CMDs) in 22 MW GCs (since that publication, a further comparison with 45 more CMDs supplied by the Panchromatic Hubble Andromeda Treasury (PHAT) project has confirmed the agreement; N. Caldwell et al. 2016, in preparation). A few metallicities from Paper II have been refined (see Table 1). The formal uncertainties in the metallicities are on average 0.15 dex; systematic uncertainties, while possibly present, should not affect our differential study here. The median velocity uncertainty for this data set is 6 km s^{-1}, as derived from clusters in common with the Strader et al. (2011) data, which had uncertainties of the order of 0.5 km s^{-1}.

We have further added a small number of new observations of previously known clusters to the collection, as well as 11 clusters discovered in the PHAT study (nearly all in the bulge, and all low-mass). No new massive GCs (above 10^5 $M_\odot$) were discovered in the NE part of the disk covered by the PHAT survey, and thus we would not expect to find many such in the SW part of the disk. The low-mass PHAT bulge clusters, those with log $M/M_\odot < 4.5$, are not included in the analysis here, because their inclusion could bias the analysis (the PHAT survey did not include the entire bulge). The complete sample is listed in Table 1. This new spectroscopic and imaging work has also resulted in us classifying a handful of other clusters as too young to be considered GCs, thus further revising some entries in Papers I and II. These are B041-G103, B255D-D072, B258, B515, and B522, all of which have ages less than 2 Gyr, based on their detailed spectra. These clusters are thus similar to the large number of disk clusters with young ages mistakenly included previously by various authors as GCs, the latest of which was Lee et al. (2008).

By combining the clusters identified as old in Papers I and II (and excluding the few just mentioned), the roughly 80 clusters

[4] The website www.cfa.harvard.edu/oir/eg/m31clusters/M31_Hectospec.html contains images, spectra and other data on all of the known M31 star clusters.

of the PAndAS survey, and the small number of bulge clusters from the PHAT survey, our best estimate of the total number of known true GCs in M31 is currently 441. Previous claims of more than 600 clusters were due to contamination by a large number of young disk clusters (Morrison et al. 2004; Puzia et al. 2005 and Lee et al. 2008). The optical disk of M31 is roughly 21 kpc in radius (down to an r-band surface brightness of 24 mag arcs^{-2}; Kent 1987), within which there are 361 old GCs (we exclude eight clusters associated[5] with NGC 205). Here are the sample sizes, where we express the number of clusters with log $M/M_{\odot} > 4.5$ in parentheses. We have velocities for 344 (336) of these clusters, and metallicity estimates, either from the spectra, colors or CMDs for 346 (336), the vast majority coming from the uniform Hectospec study. The sample that has both velocities and metallicities has 338 (332) members. Thus, our velocity and metallicity completeness within the 21 kpc radius is 94%. Our analysis here does not include the ∼80 halo clusters beyond 21 kpc. We refer the reader to Huxor et al. (2014) and Veljanoski et al. (2014) for that discussion. With this large and relatively uncontaminated sample, we hope to provide a more definitive analysis of the kinematics of the M31 GCs as a function of metallicity grouping—similar to the analysis of Elson & Walterbos (1988), but with spectroscopic rather than photometric metallicities.

We assume a distance of 770 kpc (Freedman & Madore 1990), so that $1' = 0.22$ kpc. We adopt an inclination of 77°, a minor axis position angle of −52.°3, a projected disk ellipticity of 0.7 in the outer parts (between 10 and 90′), an optical disk scale length of 27′ (6 kpc; Kent 1987), and a projected bulge ellipticity of 0.3. We will occasionally use an X–Y coordinate system for distance along the major and minor axes, with positive X and Y NE and NW of the center, respectively (e.g., M32 has negative X and Y coordinates).

3. SPATIAL PROPERTIES

In the MW, it is relatively straightforward to study the GC subpopulations and their properties, such as their spatial distributions and kinematics, owing to their clear bimodality in metallicity—with peaks near [Fe/H] = −1.6 and −0.6.

For M31, we first examine the distribution of [Fe/H] versus galactocentric radius. This is a standard approach (e.g., Barmby et al. 2000; Paper II), but normally uses a simple circular radius —as would be appropriate for a spherical system. If instead some subset of the GCs resides in an inclined, disk-like distribution, then it could be identified more clearly if disk coordinates were employed. This is done by using disk isophote parameters from the previous section to map the GCs to the semimajor axis radius R_a, where

$$R_a = R[(1 + (q^2 - 1)\cos^2\phi)^{1/2}]/q \quad (1)$$

and R is the distance to the galaxy center (taken to be R.A. = 0:42:44.3 decl. = +41:16:09.4), $q = 0.3$, the ratio of the assumed axes, and ϕ is the angle the cluster makes with respect to the major axis and the center. The R and R_a values are also tabulated in Table 1.

Figure 1 shows the results: clusters more metal-rich than [Fe/H] = −0.4 are not found outside of $R_a = 8$ kpc. The same radius marks an apparent distinction in the density of GCs

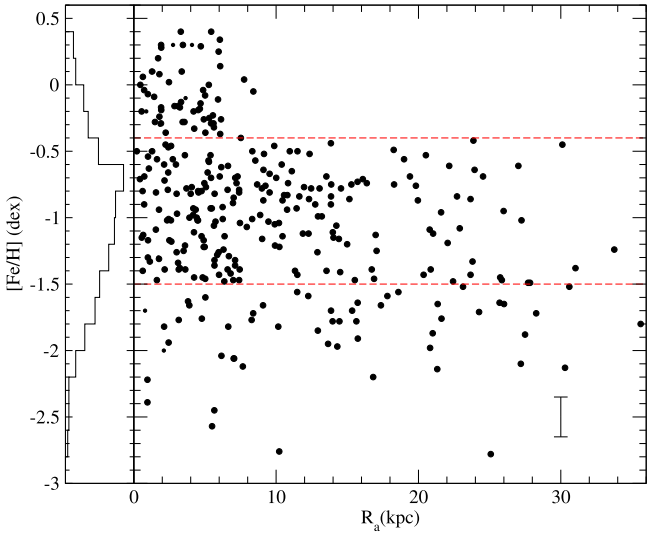

Figure 1. Distribution of M31 GC iron metallicity with semimajor axis radius, projected elliptically to the disk. In this plot, three metallicity groups emerge (with divisions at [Fe/H] ∼ −0.4 and −1.5, shown as dashed lines), based on their relative densities inside and outside a disk radius of ∼8 kpc. Note that 8 clusters around NGC 205 (at R_a = 24–28 kpc) have been removed from this plot, and there are also another 115 GCs (mostly from the PAndAS survey) that either have no known metallicity or extend off the plot to larger radii. Ten clusters with log mass in solar units less than 4.5 are shown as smaller dots (mostly at small radii). As a result, there are 326 clusters shown here. The median metallicity uncertainty of ±0.15 dex is shown by error bars at the lower right. The binned metallicity distribution among all of clusters (including those off the radius scale) is shown at the left, reiterating the finding in Caldwell et al. (2011) that the distribution is not simply bimodal.

above and below [Fe/H] ∼ −1.5, with relatively few of the more metal-poor objects found at smaller radii. These are the same metallicity divisions previously found in Paper II, and are also visible, though less clearly, when using bulge coordinates or simple radial coordinates.

To better isolate these transitions, we calculate the half-number radius for groups of GCs in different metallicity bins—i.e., the radius that divides a group in half (again we leave out the smaller PHAT clusters). For the overall sample of GCs within a limiting radius of R = 21 kpc (with median [Fe/H] = −1.0), that half-number radius is $R = 4.2$ kpc. For the 56 GCs with [Fe/H] ⩾ −0.4 (and median [Fe/H] = −0.1), it is much smaller, $R = 1.9$ kpc. The 59 GCs with [Fe/H] < −1.5 (median [Fe/H] = −1.9) have a much larger half-number radius of $R = 6.3$ kpc. Here we have experimented with different metallicity boundaries and thereby found these values where the derived radius shows a transition—both for the disk radius and for the normal projected radius—noting again that the uncertainty in metallicity for individual clusters is around 0.15 dex. The 223 GCs at intermediate metallicity (median [Fe/H] = −1.0) have a half-number radius of $R = 4.2$ kpc, in between the values of the metal-rich and metal-poor groups.

4. KINEMATICS OF DIFFERENT METALLICITY GROUPS

We now investigate how the two metallicity dividing lines play out in the M31 cluster kinematics. Figure 2 shows the GC velocities relative to the mean M31 velocity (−300 km s^{-1}), with a sign inversion for clusters on opposite sides of the

[5] These are B009-G061, B011-G063, B317-G041, B328-G054, B330-G056, B331-G057, B333, and BH04.

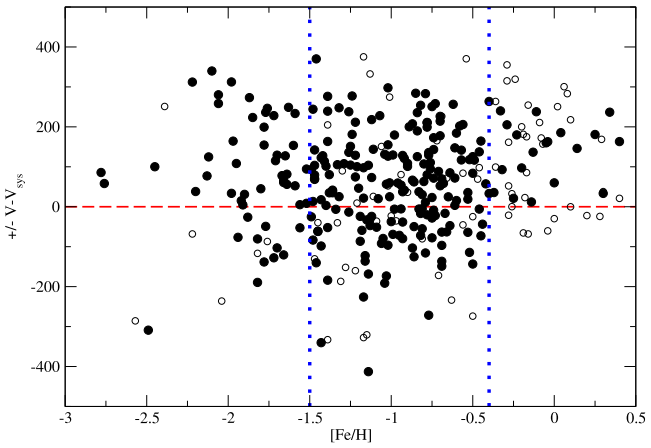

Figure 2. Second diagnostic plot outlining M31 GC metallicity groups. Here, velocity with respect to systemic velocity, with a sign inversion on opposite sides of the rotating disk, is plotted against [Fe/H]. Thus, objects with positive ordinate values are rotating prograde; retrograde velocities result in negative ordinate values. Clusters closer than 2 kpc to the center are shown as open circles; those farther out are shown as filled circles. This plot again suggests that clusters can be divided at [Fe/H] = −0.4 and [Fe/H] = −1.5, shown by the dotted vertical lines. Nearly all clusters more metal-rich than [Fe/H] = −0.4 have prograde motions. Lower metallicity clusters have roughly twice as many prograde as retrograde clusters, indicating systemic rotation for them.

rotating disk, plotted against the cluster metallicity. That is, for GCs on the approaching SW side, $-(V-V_{\rm sys})$ is plotted, while on the NE, receding side, $(V-V_{\rm sys})$ is plotted. In such a plot, prograde velocities will always be positive, while retrograde will be negative. Viewed in this manner, in all three metallicity groups, there is net rotation in the same direction. More than 90% of clusters more metal-rich than [Fe/H] = −0.4 clearly have prograde motion—and no metal-rich cluster outside of 2 kpc has retrograde motion. These facts imply disk kinematics for the most metal-rich clusters. For the intermediate metallicity and metal-poor clusters, about 1/3 of the clusters have retrograde motions. Excluding the inner 2 kpc objects, we find that again 1/3 of the intermediates have retrograde motion, while only 1/5 of the metal-poor clusters have retrograde motion. It is no surprise that these groups are not purely disk systems, but there is clearly some rotation, which we take up below. Allen et al. (2006, 2008) studied the orbits of 54 MW GCs, 32 of them more metal-poor than [Fe/H] = −0.8 (the inflection point of the MW metallicity distribution) and found that half of those metal-poor clusters are on retrograde orbits, a much larger fraction than found in M31.

Figure 3 shows those three groups in a composite image, where the positions in M31 are shown, along with their color-coded velocities. Our metallicity divisions are sharp, and do not account for uncertainties in the metallicities, but the general characteristics of this plot remain unchanged if we modify the group boundaries. For the most metal-rich clusters, with [Fe/H] > −0.4, we find that all but one of these 56 clusters are confined to the disk light distribution. The cluster concentration, noted above, is quite apparent, as is the systemic rotation, and as we reported in Morrison et al. (2011), the metal-rich clusters with $R < 2$ kpc have apparent strong rotation, likely indicating a response to a bar potential. Just as apparent, clusters with [Fe/H] < −1.5 are not concentrated, and are more spherically distributed, in projection. Within 2 kpc, there are only 7 clusters in our metal-poor group[6], whereas each of the other 2 groups has roughly 40. Even in this qualitative plot, one can see that all three metallicity groups have some degree of rotation, though not nearly as strong as reported in earlier papers cited above.

The positions of MW clusters are plotted on the right side of this figure, in similar metallicity groups, but with different specific dividing lines. The positions were determined from the galactic *XYZ* coordinates in kiloparsecs provided in the Harris (1996) MW GC catalog from 2010, where we have projected those as follows: $X' = ((X - R_\odot)^2 + Y^2)^{1/2}$ and $Y' = Z$, where $R_\odot = 8$ kpc. We grouped these in the following metallicity bins: [Fe/H] > −1.0, −1.5 > [Fe/H] > −1.0, and [Fe/H] < −1.5. The first group includes clusters more metal-rich than the saddle point in the overall distribution, while the second and third groups divide the remainder at about the peak of the metal-poor grouping. As has been pointed out many times previously (e.g., Zinn 1996), the metal-rich group has a large mean rotational velocity, a small line of sight dispersion, and a flattened spatial distribution. The most metal-poor MW group again shows much less concentration than do the other two metallicity bins. We cannot show velocities in the MW plot, but recall that the metal-poor MW clusters do not show bulk rotation (Harris 2001: $v/\sigma \sim 0.25$, where σ is the group velocity dispersion), unlike those in M31.

To provide some numbers on the bulk rotation, we analyze the M31 GC radial velocities as a function of position angle with respect to the minor axis of M31 (taken to be at a position angle of $-52\overset{\circ}{.}3$). We fit a simple sine function to these data using non-linear least squares (see Sharples et al. 1998)

$$V(\theta) = V_0 + K \sin(\theta - \theta_0), \quad (2)$$

where $V(\theta)$ is the cluster observed radial velocity at position angle θ, V_0 is the group mean velocity, K is the amplitude of rotation, and θ_0 is the position angle of the axis of rotation.[7] We fit each of our three defined metallicity groups separately, and derived the dispersions about those fits (see Figure 4). The results are presented in Table 2, where we have further broken up the metal-rich sample into bulge and non-bulge clusters (those with $R > 2$ kpc). The non-bulge metal-rich group has a bulk rotation rate of around 160 km s^{-1}, with a moderate dispersion of 80 km s^{-1} ($v/\sigma \sim 2.0$). The intermediate-metallicity group has a rotation of 53 km s^{-1}, and a dispersion of 141 km s^{-1} ($v/\sigma \sim 0.4$), while the metal-poor group has a somewhat higher rotation of 90 km s^{-1}and a similar dispersion of 154 km s^{-1} ($v/\sigma \sim 0.6$). The detected bulk rotation rates are significantly non-zero for the intermediate and metal-poor groups, 4.0σ and 3.8σ, respectively (from Table 2, where σ here is the uncertainty in the derived parameter). Similar results are found if we fix the mean velocity of all the subgroups to be equal to that of the full group.

For the metal-rich group, we can also compare the observed radial velocities with those expected for the thin disk at those positions, using the H I+H II-based rotation model of Kent (1989), and derive a dispersion from the differences. The rotation model uses a major axis curve that rises linearly to

[6] These are AP8925, B041D, B086-G148, B114-G175, B157-G212, B165-G218, and B264-NB19.

[7] We have also experimented with fits that include azimuthal flattening, equivalent to tilted-ring models (e.g., Foster et al. 2011), and find similar results, though with somewhat stronger rotation.

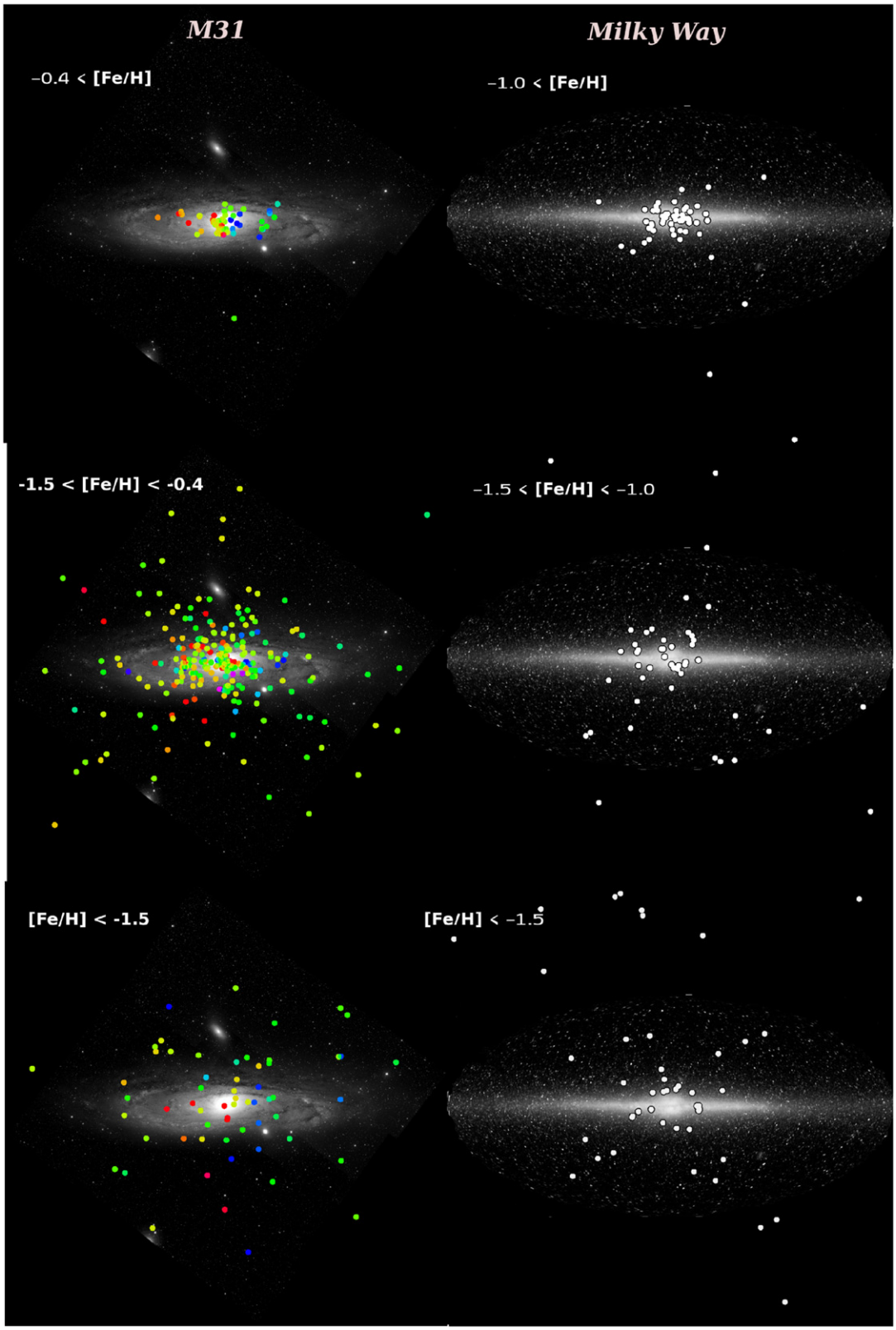

Figure 3. Left panels: maps of the locations of different [Fe/H] groups for M31 GCs, color-coded by velocity. In the upper plot are the most metal-rich, [Fe/H] > -0.4. The middle plot shows clusters with $-0.4 <$ [Fe/H] < -1.4, while the lower panel contains the most metal-poor group. The background image is from the DSS, where the field size is 50 kpc. The color-coding is with respect to the mean M31 velocity, and is as follows: violet $= -375$, blue $= -275$, green $= -100$, yellow $= -50$, orange $= -150$ and red $= +225$ km s^{-1}. The most metal-poor group is much less concentrated than the metal-rich group. The outlying cluster in the metal-rich group is B379-G312, discussed in the text. Right panels: similar plots for MW clusters, where the projection of galactic *XYZ* onto a plane is described in the text. At the top are the most metal-rich clusters, with [Fe/H] > -1.0, which represents the clusters of the metal-rich peak in the overall metallicity distribution. The middle panel shows clusters with $-1.0 <$ [Fe/H] < -1.5, and the bottom has clusters with [Fe/H] < -1.5. The dividing line here is at the peak of the metal-poor group in the MW. The background image is the DIRBE/COBE image of the MW (courtesy NASA & E. Wright). We arbitrarily set the MW image to be 40 kpc in diameter for this display, similar to the size of the image shown of M31. Like the situation for M31, the metal-poor MW clusters show less concentration than the metal-rich group. As general information, this plot also shows that M31 has 361 known GCs within a projected radius of 21 kpc, while the MW has just 129.

Table 2
Rotation of Different Metallicity Groups[a]

Group	N	V_0 km s^{-1}	K km s^{-1}	θ_0[b] Deg.	σ km s^{-1}
All, $R < 21$ kpc, Log $M/M_\odot < 4.5$	332	-301 ± 8	80 ± 10	89 ± 9	140
$-0.4 <$ [Fe/H]	54	-302 ± 14	168 ± 16	89 ± 9	104
$-0.4 <$ [Fe/H], $R < 2$	33	-315 ± 24	195 ± 31	87 ± 9	120
$-0.4 <$ [Fe/H], $2 < R < 21$	20	-292 ± 18	160 ± 35	113 ± 25	80
$-1.5 <$ [Fe/H] < -0.4	221	-299 ± 10	53 ± 13	101 ± 16	141
$-1.5 <$ [Fe/H] < -0.4, $\lvert Y\rvert < 4$ kpc	162	-304 ± 12	53 ± 17	108 ± 22	152
[Fe/H] < -1.5	57	-309 ± 20	90 ± 23	71 ± 24	154
[Fe/H] < -1.5, $\lvert Y\rvert < 4$	27	-285 ± 29	112 ± 42	51 ± 31	154

Notes.
[a] Uncertainties were determined by a bootstrap method.
[b] 90° is the photometric minor axis.

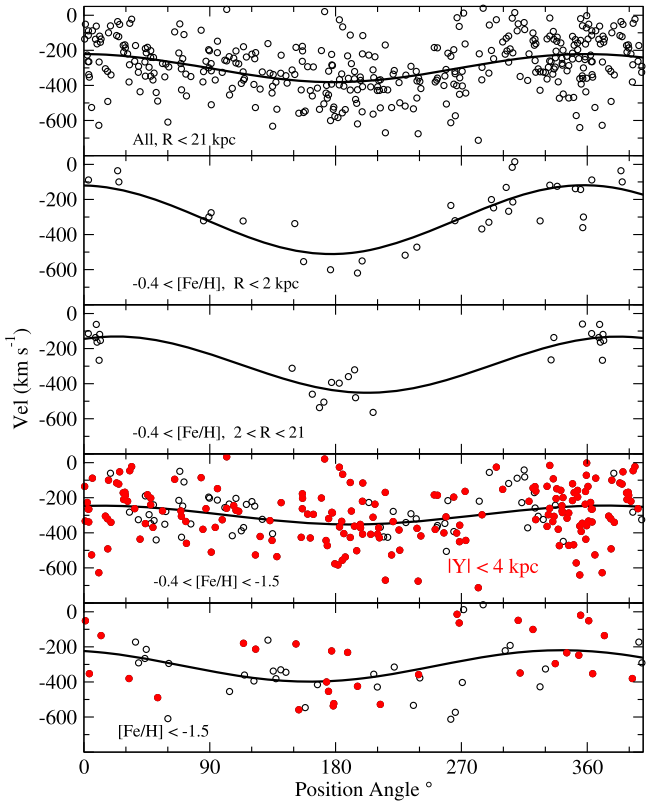

Figure 4. Radial velocity plotted as a function of position angle with respect to the minor axis, in metallicity and radius bins. Curves show model fits for mean velocity vs. position angle. All data refer to clusters with radius <21 kpc. At the top are plotted all such clusters, demonstrating that the entire sample has bulk rotation at the level of 80 km s^{-1}, shown as the continuous line. Table 2 lists the derived values for all the subgroups shown. In the lower two panels, filled red circles refer to clusters projected to within 4 kpc of the stellar disk, to search more closely for disk-like rotation in these two more metal-poor groups.

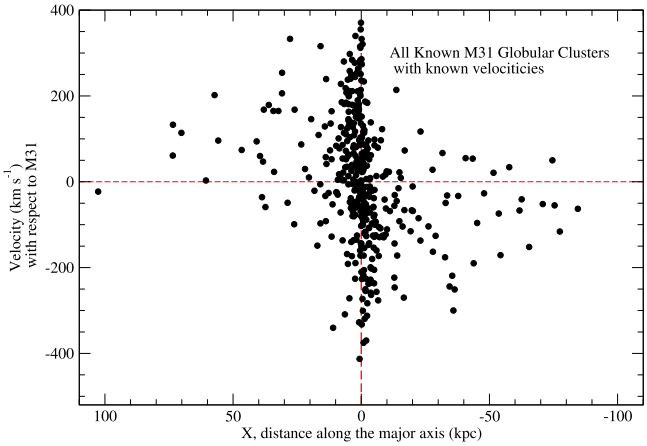

Figure 5. Radial velocity plotted as a function of projected distance along the major axis (X), for all M31 GCs without radius restriction, with measured velocities (421 out of the full 441 M31 GCs that we have collected), including the outer clusters discussed in Veljanoski et al. (2014). The outer clusters (those with $X > 21$) do show the same sense of rotation as the inner ones, as reported, but the version of the inner data shown in that paper was contaminated by young disk clusters. Dashed lines show the zero levels for both axes.

250 km s^{-1} out to a radius of 6.5 kpc, and is flat outside of that. Projected velocities throughout the disk are then given by $V = V_{\rm rot} \cos\theta \sin i$, where $V_{\rm rot}$ is the major axis rotation at the distance corresponding to the location of the GC, θ is the angle with respect to the major axis, and i is again the inclination. Again, we find a dispersion about the thin disk rotation of 80 km s^{-1} for the metal-rich group. A similar result is derived if we use the actual M31 H I velocity map of C. Lee & A.K. Leroy (2016, private communication), though not all clusters have H I detected at their location. It is to be expected that these old clusters would have higher dispersions than a thin disk of H I gas.

The dispersion in 140 H II region velocities about the disk model as derived from the data presented in Sanders et al. (2012) is about 50 km s^{-1}. From the data in Paper I we can also derive the dispersion of the diffuse disk gas (from 60 pointings), and that of 60 clusters younger than 1 Gyr. Those values are 39 and 41 km s^{-1}, respectively. Another comparison can be made to results from the Spectroscopic and Panchromatic Landscape of Andromeda's Stellar Halo Survey (Dorman et al. 2012, 2013, 2015). Here the kinematics of individual RGB stars have been analyzed and separated into disk and spheroid components. In the same radial range as the metal-rich GCs, the disk stars have velocity dispersions of ~90–130 km s^{-1}, while the spheroid has a dispersion of ~120–160 km s^{-1}. Thus, the metal-rich GCs appear to track the galaxy disk rather than the spheroid (or extended bulge).

The two more metal-poor GC metallicity groups also have mild systemic prograde rotation, though with larger dispersions. Their ~50–100 km s^{-1} rotation is lower than the ~120–200 km s^{-1} values that have been circulating in the literature for the past decade. Our revised value also matches up nicely with the outer halo rotation of ~80 km s^{-1}, which had previously shown a peculiar disconnect with the inner halo (see Figure 2 from Veljanoski et al. 2013 and Figure 7 from Veljanoski et al. 2014), owing to the inner GC sample being contaminated with very young clusters. Our updated summary of all available M31 GC velocities, out to ~100 kpc, is shown in Figure 5.

Relating back to the field star components again, the intermediate-metallicity GCs are kinematically similar to the RGB extended spheroid stars, but have a lower metallicity (median [Fe/H] ~ -1.0 versus -0.5; Gilbert et al. 2014). Instead, they may be associated with the metal-poor "halo" detected through RGB stars (Gilbert et al. 2012; Ibata et al. 2014). The most metal-poor GC group has higher rotation than the intermediate group, and is spatially the least concentrated of the three groups, by a factor of at least five within a radius of 2 kpc, as calculated from the positions listed in Table 1. Again, it may be associated with the RGB halo, and we note that the presence of a metal-poor stellar halo in M31, and in many other galaxies, was evident from the GCs, long before resolved field-star studies were feasible.

There is some asymmetry in the bulk rotation patterns of the GCs to comment on. For instance, the minimum observed radial velocity of unresolved optical light on the approaching side (SW, negative X, right side of the M31 image in Figure 3) is about -250 km s^{-1} (relative to systemic; from data reported in Paper I). The maximum velocity on the receding side (NE, positive X, left side) is about $+350$ km s^{-1}. There are no clusters on the approaching side with velocities greater than $+200$ km s^{-1} which are farther than 1 kpc from the center (i.e., with velocities that differ from the local disk velocity by $+450$ km s^{-1}), but there are four clusters on the receding side with velocities less than -200 km s^{-1} (-450 km s^{-1} with respect to the local disk), three of them projected on the disk. These are V129-BA4, B213-B264, and B173-G224. There is nothing else unusual about these clusters, but again perhaps more detailed analysis is warranted to see if they were deposited by the Giant Southern Stream or another stream.

One metal-rich cluster, B094-G156, has an observed radial velocity that is -202 km s^{-1} different from the local disk velocity (though prograde), making its velocity difference similar to the bar-influenced clusters at smaller radii, even though it is much farther from the center (4 kpc along the minor axis) than the other such clusters reported in Morrison et al. (2011), who considered clusters within a radius of 2 kpc.

One final comment to make regarding the four metal-rich clusters with [Fe/H] ~ -0.4 that lie outside the optical disk, and at radii larger than 10 kpc, is that they are more than twice as far as the next farthest metal-rich cluster. These are B339-G077, B379-G312, B398-G341, and B407-G352. B407-G352 has been suggested as the remnant nucleus of the Giant Southern Stream (Perina et al. 2009). Perhaps the other three outer, high-metallicity clusters bear further investigation with that topic in mind.

5. SUMMARY AND DISCUSSION

We now return to comparisons of the MW and M31 GC systems (Section 1). First, as is well-known, M31 has more than twice the total number of GCs as the MW. Within the optical disks of both galaxies (using 21 kpc for both), there are 361 GCs in M31 and 129 in the MW (using Harris 1996 for the MW numbers). Larger numbers for M31 reported previously are contaminated by the inclusion of young disk clusters.

Second, while the metallicity distribution for the MW is clearly bimodal, that of M31 is not a simple superposition of Gaussians. In this paper, we have suggested three components: a very metal-rich group, the dominant intermediate-metallicity group, and a metal-poor group. These groups are most easily defined by their differing two-dimensional spatial distributions, as shown in Figure 1.

Third, outside of the central bulge regions, the metal-rich group (20 clusters) has convincing disk kinematics (both in rotation and velocity dispersion), has a spatial distribution like the optical M31 disk, and is much more concentrated than the other two GC groups. The lower-metallicity groups have weak but significant prograde rotation. The metal-poor group is the least concentrated of the three groups, down by a factor of at least five. These results obviate the need to invoke a major merger (see also Veljanoski & Helmi 2016), and they bring the properties of the M31 GC system into closer alignment with the MW. Although the numbers of GCs as a function of metallicity are different for the two galaxies, their spatial and kinematical trends with metallicity are fairly similar—as was previously emphasized by Elson & Walterbos (1988).

The clear disk-like properties of the M31 metal-rich GCs provide an important window into the formation mechanisms of both galaxies and star clusters. In the MW, the difficulties in observing the metal-rich GC sub-system lead to ambiguity in classifying them as bulge or thick-disk objects. Consequently, an association between bulges and metal-rich GCs is often assumed, along with gas-rich major mergers, as the mechanism that formed these GCs (e.g., Ashman & Zepf 1992; Li & Gnedin 2014). This picture has been tested recently in lenticular galaxies through detailed comparisons of metal-rich GCs to the bulge and disk field-star components (Forbes et al. 2012; Cortesi et al. 2016), with mixed results. However, the case of M31 highlights an alternative to the merger scenario: that a population of GCs formed in situ, within giant star-forming clumps in turbulent galactic disks at high redshifts (Shapiro et al. 2010; Kruijssen 2015).

Although this disk mode of GCs is intriguing, the very dominant subpopulations in M31 are the lower-metallicity GCs. It seems likely that these objects were brought in by the accretion of satellite galaxies (minor mergers). The populous GC system of M31, relative to the MW, would then reflect a more active accretion history, and the radial gradient of GC metallicities could arise through correlations of both metallicity and dynamical friction with satellite galaxy mass (e.g., Amorisco 2016).

The chemodynamical structure of M31, and its assembly history, could be clarified in the future by comparing the GCs to the stars in more detail. Analysis of additional spiral galaxies and their GC systems may also reveal how pervasive the different modes of GC formation are, and how representative M31 and the MW are of other galaxies.

Important discussions were had with Jay Strader, Anil Seth, Ricardo Schiavon, Heather Morrison, and Claire Dorman. We thank Adam Leroy and Cheoljong Lee for the use of the M31 HI map.

REFERENCES

Allen, C., Moreno, E., & Pichardo, B. 2006, ApJ, 652, 1150
Allen, C., Moreno, E., & Pichardo, B. 2008, ApJ, 674, 237
Amorisco, N. C. 2016, MNRAS, submitted (arXiv:1511.08806)
Ashman, K. M., & Zepf, S. E. 1992, ApJ, 384, 50
Barmby, P., Huchra, J. P., Brodie, J. P., et al. 2000, AJ, 119, 727
Beasley, M. A., Brodie, J. P., Strader, J., et al. 2004, AJ, 128, 1623
Bekki, K. 2010, MNRAS, 401, L58
Caldwell, N., Harding, P., Morrison, H., et al. 2009, AJ, 137, 94
Caldwell, N., Schiavon, R., Morrison, H., Rose, J. A., & Harding, P. 2011, AJ, 141, 61
Carollo, D., Beers, T. C., Lee, Y. S., et al. 2007, Natur, 450, 1020
Cezario, E., Coelho, P. R. T., Alves-Brito, A., Forbes, D. A., & Brodie, J. P. 2013, A&A, 549, A60
Colucci, J. E., Bernstein, R. A., & Cohen, J. G. 2014, ApJ, 797, 116
Cortesi, A., Chies-Santos, A. L., Pota, V., et al. 2016, MNRAS, 456, 2611
Deason, A. J., Belokurov, V., & Evans, N. W. 2011, MNRAS, 411, 1480
Dorman, C. E., Guhathakurta, P., Fardal, M. A., et al. 2012, ApJ, 752, 147
Dorman, C. E., Guhathakurta, P., Seth, A. C., et al. 2015, ApJ, 803, 24
Dorman, C. E., Widrow, L. M., Guhathakurta, P., et al. 2013, ApJ, 779, 103
Elson, R. A., & Walterbos, R. A. M. 1988, ApJ, 333, 594
Fabricant, D., Fata, R., Roll, J., et al. 2005, PASP, 117, 1411
Forbes, D. A., & Bridges, T. 2010, MNRAS, 404, 1203
Forbes, D. A., Cortesi, A., Pota, V., et al. 2012, MNRAS, 426, 975
Foster, C., Spitler, L. R., Romanowsky, A. J., et al. 2011, MNRAS, 415, 3393
Freedman, W. L., & Madore, B. F. 1990, ApJ, 365, 186
Freeman, K. C. 1983, in IAU Symp. 100, Internal kinematics and dynamics of galaxies, ed. E. Athanassoula (Dordrecht: Reidel), 359
Galleti, S., Bellazzini, M., Buzzoni, A., Federici, L., & Fusi Pecci, F. 2009, A&A, 508, 1285
Galleti, S., Bellazzini, M., Federici, L., Buzzoni, A., & Fusi Pecci, F. 2007, A&A, 471, 127
Gilbert, K. M., Guhathakurta, P., Beaton, R. L., et al. 2012, ApJ, 760, 76
Gilbert, K. M., Kalirai, J. S., Guhathakurta, P., et al. 2014, ApJ, 796, 76
Harris, W. E. 1996, yCat, 7195, 0
Harris, W. E. 2001, in Saas-Fee Advanced Course 28, Swiss Society for Astronomy and Astrophysics, ed. L. Labhardt, & B. Binggeli (Berlin: Springer), 223
Huchra, J., Stauffer, J., & van Speybroeck, L. 1982, ApJL, 259, L57
Huchra, J. P., Brodie, J. P., & Kent, S. M. 1991, ApJ, 370, 495
Huxor, A. P., Mackey, A. D., Ferguson, A. M. N., et al. 2014, MNRAS, 442, 2165
Ibata, R. A., Lewis, G. F., McConnachie, A. W., et al. 2014, ApJ, 780, 128
Keller, S. C., Mackey, D., & Da Costa, G. S. 2012, ApJ, 744, 57
Kent, S. M. 1987, AJ, 94, 306
Kent, S. M. 1989, PASP, 101, 489
Kruijssen, J. M. D. 2015, MNRAS, 454, 1658
Lee, M. G., Hwang, H. S., Kim, S. C., et al. 2008, ApJ, 674, 886
Li, H., & Gnedin, O. Y. 2014, ApJ, 796, 10
Mackey, A. D., & Gilmore, G. F. 2004, MNRAS, 355, 504
Mackey, A. D., Huxor, A., Ferguson, A. M. N., et al. 2006, ApJL, 653, L105
Mackey, A. D., Huxor, A., Ferguson, A. M. N., et al. 2007, ApJL, 655, L85
Mackey, A. D., Huxor, A. P., Ferguson, A. M. N., et al. 2013, MNRAS, 429, 281
McCarthy, I. G., Font, A. S., Crain, R. A., et al. 2012, MNRAS, 420, 2245
McConnachie, A. W., Irwin, M. J., Ibata, R. A., et al. 2009, Natur, 461, 66
Morrison, H., Caldwell, N., Schiavon, R. P., et al. 2011, ApJL, 726, L9
Morrison, H. L., Harding, P., Perrett, K., & Hurley-Keller, D. 2004, ApJ, 603, 87
Morrison, H. L., Helmi, A., Sun, J., et al. 2009, ApJ, 694, 130
Perina, S., Federici, L., Bellazzini, M., et al. 2009, A&A, 507, 1375
Perina, S., Galleti, S., Fusi Pecci, F., et al. 2011, A&A, 531, A155
Perrett, K. M., Bridges, T. J., Hanes, D. A., et al. 2002, AJ, 123, 2490
Puzia, T. H., Perrett, K. M., & Bridges, T. J. 2005, A&A, 434, 909
Rich, R. M., Corsi, C. E., Cacciari, C., et al. 2005, AJ, 129, 2670
Sanders, N. E., Caldwell, N., McDowell, J., & Harding, P. 2012, ApJ, 758, 133
Searle, L., & Zinn, R. 1978, ApJ, 225, 357
Shapiro, K. L., Genzel, R., & Förster Schreiber, N. M. 2010, MNRAS, 403, L36
Sharples, R. M., Zepf, S. E., Bridges, T. J., et al. 1998, AJ, 115, 2337
Strader, J., Caldwell, N., & Seth, A. C. 2011, AJ, 142, 8
Veljanoski, J., Ferguson, A. M. N., Mackey, A. D., et al. 2013, ApJL, 768, L33
Veljanoski, J., & Helmi, A. 2016, A&A, submitted (arXiv:1602.04018)
Veljanoski, J., Mackey, A. D., Ferguson, A. M. N., et al. 2014, MNRAS, 442, 2929
Zinn, R. 1985, ApJ, 293, 424
Zinn, R. 1996, in ASP Conf. Ser. 92, Formation of the Galactic Halo…Inside and Out, ed. H. Morrison, & A. Sarajedini (San Francisco: ASP), 211